

Introduction to microseismic source mechanisms

Rie Kamei¹, Nori Nakata², and David Lumley¹

Microseismic events are very weak earthquakes that occur at very small spatial scales. Microseismic events can result from natural forces such as tectonic motions (natural seismicity) or they can be induced by man-made changes to the natural stress-strain conditions in the earth (induced seismicity). There is a growing awareness that fluid injection into or fluid withdrawal from the earth's subsurface (e.g., oil/gas production, geothermal energy production, waste-fluid disposal), which changes the pore pressure, stress, and strain conditions in the rock, can induce microseismic events and might eventually lead to larger "felt" seismic events. (See the June 2015 *TLE* special section on injection-induced seismicity.)

In the past decade, analysis of passive recordings of microseismic data and location of detected microseismic sources has led to an improved understanding of fracture and fault behavior. In this special section, we focus on the analysis of microseismic source mechanisms, which goes beyond the traditional location and timing of microseismic events to determine the source waveforms and radiation patterns at each microseismic source location. This analysis provides more in-depth information about the in situ stress and strain conditions and the local subsurface geomechanical properties and forces at work.

Microseismicity

In the earthquake-seismology community, a microseismic event typically is defined as an earthquake that is not "felt" by the public, which usually implies an earthquake with a "moment magnitude" M_W less than about 3 or 4. M_W is a common measure of an earthquake's strength and is a dimensionless quantity defined as $M_W = 0.67 \log_{10}(M_0) - 6.07$.

In the equation above, the variable M_0 is the "seismic moment" in units of $[N \cdot m]$, which is a quantitative measure of the amount of energy released in an earthquake such that $M_0 = \mu A D$, where A is the surface area of the rupture created by the earthquake along a fault or fracture, D is the amount of rock displacement along the rupture surface, and μ is the average shear strength of the rock encompassing the ruptured zone. A fracture is defined as a crack or break in a rock, and a fault is defined as a fracture along which relative displacement or "throw" of the rock has occurred across the fracture.

For typical fluid injection or withdrawal scenarios, reservoir pressure changes of a few hundred psi (a few megapascals) can induce weak microseismic events of magnitudes less than $M -2$, with associated rock displacements much less than a millimeter along fracture scale lengths much shorter than a meter. An $M -2$ event is approximately one billion times weaker (less energetic) than earthquakes that the public can feel. Moderate "fault reactivation" or significant "rock-fracturing" events typically induce microseismic energy of magnitudes less than $M2$, with associated rock displacements less than a centimeter along fracture or fault lengths shorter than a few (or tens of) meters. An $M2$ event is approximately 100

to 1000 times weaker than what the public can feel. Large fault-related earthquake rupture events typically radiate seismic energy with magnitudes greater than $M4$, with associated fault slip displacements greater than several centimeters or meters along fault lengths greater than several (tens or hundreds of) kilometers. An $M3$ or $M4$ event is typically the weakest magnitude that the public can feel.

Figure 1 compares an induced microseismic waveform ($M < 0$) with a natural felt earthquake ($M > 5$). The microseismic waveform contains much higher-frequency content than the earthquake waveform. Larger earthquakes have rupture processes of greater duration (tens of seconds to minutes), which tends to suppress higher-frequency components (e.g., Haskell fault model). The corresponding cutoff frequency or corner frequency is generally inversely proportional to earthquake size. Microseismic data are characterized by smaller magnitudes, higher frequencies, shorter wavelengths, and shorter duration. Conversely, most felt earthquake data are characterized by larger magnitudes, lower frequencies, longer wavelengths, and longer duration. Based on scaling relationships between various source parameters (including frequency content and magnitude), processing techniques developed for natural felt earthquakes have been applied to microseismic data.

Microseismic monitoring is an important tool for monitoring fluid flow and pressure/stress changes in the subsurface during fluid injection and extraction, especially during hydraulic fracturing for enhanced hydrocarbon production and geothermal energy production. In general, we record the seismic waves generated by microseismic events with geophone arrays at or near the earth's surface and in boreholes. Because we cannot predict the exact source-excitation times of microseismic events, we measure ground motion continuously and try to detect microseismic waveforms in the continuous recorded data. For all microseismic events detected, we locate the (x, y, z) spatial location (hypocenter) and the

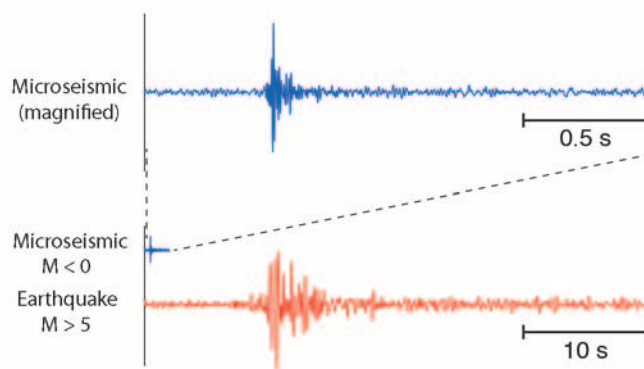


Figure 1. Example of recorded seismic waveforms generated by an $M_W < 0$ induced microseismic event (blue) and an $M_W > 5$ natural felt earthquake (red).

¹Perth, Australia.

²Stanford, California.

source time t_0 for each event. The microseismic-event locations tell us about the region of fluid flow, pressure change, and rock fracturing. If we know the location of preexisting faults in the area, we can discriminate which events are related to fault reactivation. From the locations of events alone, we cannot readily estimate the mechanism of rock failure, quantitative stress-strain changes, event magnitude, the slip zone and direction of slip, or the in situ geomechanical properties. However, we can estimate this information through analysis of the source mechanisms. Next, we briefly discuss how geomechanical stress-strain principles are related to the generation of seismic waves caused by rock failure and the determination of seismic source mechanisms.

Seismic source mechanisms

Stress is defined as the force per unit area applied to the surface of a solid material. We can define a stress tensor σ_{ij} ($i = x, y, z, j = x, y, z$) in a Cartesian coordinate system (Figure 2 in the xy -plane), where σ_{ii} are the compressive stresses normal to the surface and τ_{ij} are the shear stresses parallel to the surface. To balance the torque applied to the material (i.e., assuming the material is irrotational), the shear stresses must be symmetrical ($\tau_{xy} = \tau_{yx}$, $\tau_{yz} = \tau_{zy}$, $\tau_{zx} = \tau_{xz}$), and thus the stress tensor has six independent stress components (σ_{xx} , σ_{yy} , σ_{zz} , τ_{xy} , τ_{yz} , τ_{zx}). Because the tensor is symmetrical, we can make the shear stress zero by rotating the coordinate system (e.g., by eigenvector analysis). This special direction is called the principal stress orientation and is described by three normal components ($\sigma_1 > \sigma_2 > \sigma_3$), where σ_1 is the maximum principal stress and σ_3 is the minimum principal stress.

The state of stress and rock failure in a solid medium can be described by the Mohr circle diagram and the Mohr-Coulomb-Griffith failure criterion (Figure 3). The Mohr circle is a 2D illustration of the stress tensor in the normal stress (horizontal axis) and shear stress (vertical axis) domains. The black Mohr circle in Figure 3 indicates an initial stable stress condition, and each point along the Mohr circle corresponds to the normal and shear stress values at various coordinate direction rotation angles. For example, the stress values along the horizontal axis describe the minimum and maximum principal stresses because the shear stress is zero. Note that the stress values plotted in the Mohr circle diagram are *effective*-stress values, i.e., the applied stress minus the pore pressure. The initial stable Mohr circle can be shifted toward the failure envelope by changing either the applied stress or the pore pressure (e.g., by fluid injection or withdrawal).

The slope of the Mohr-Coulomb-Griffith failure envelope is related to the sliding friction of the rock material, and the intercept is related to the cohesion or fracture strength of the rock. The rock “fails” (i.e., fractures or slips) when the Mohr circle touches or crosses the Mohr-Coulomb-Griffith failure envelope. This rock failure and stress release are the energy source that generates seismic waves. The fracture angle of the rock failure is given by the angle perpendicular to the failure envelope at the point where the Mohr circle touches the failure envelope. For example, failure can be induced by an increase in maximum principal stress (e.g., long-term tectonic deformation; blue circle

in Figure 3) or an increase in pore pressure (e.g., water injection; red circle in Figure 3). A failure occurring in the positive normal stress region represents a shear failure (right inset in Figure 3), while one in the negative normal stress region represents a tensile failure (left inset in Figure 3). Because of the shape of the failure envelope, the tensile failure radiates smaller energy than the shear failure. Thus, the magnitude of tensile earthquakes is generally smaller, and the radiated seismic waves contain higher-frequency contents.

Depending on the ratio of the principal stresses, pure shear failure is classified into three stress-strain regimes: strike-slip, normal slip, and reverse slip (Figure 4). The vertical stress

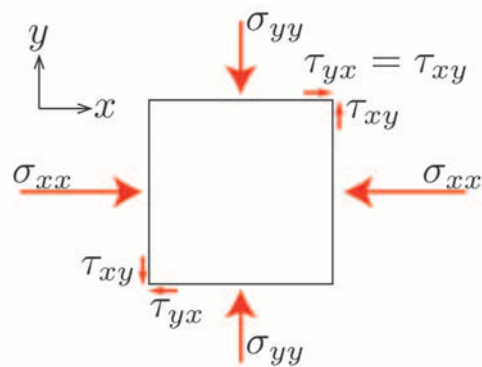


Figure 2. Normal (σ) and shear (τ) stress components on the xy -plane of a solid surface.

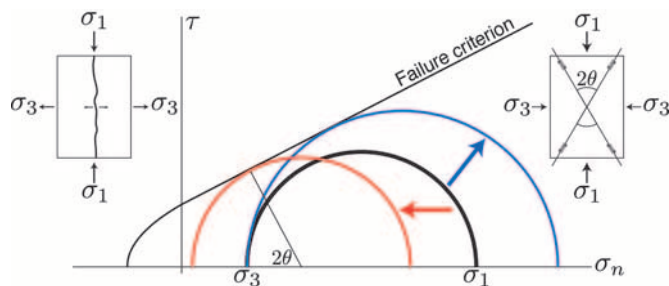


Figure 3. Mohr circle diagram with the Mohr-Coulomb-Griffith failure-criterion envelope. The horizontal axis is effective normal stress; the vertical axis is effective shear stress. The black Mohr circle illustrates a stable stress condition, and the red and blue Mohr circles indicate examples of stress-induced failure conditions. θ is the angle of the failure plane. The schematic insets show the resulting fracture mechanisms: (right) pure shear failure (positive normal stress regime) and (left) pure tensile failure (negative normal stress regime).

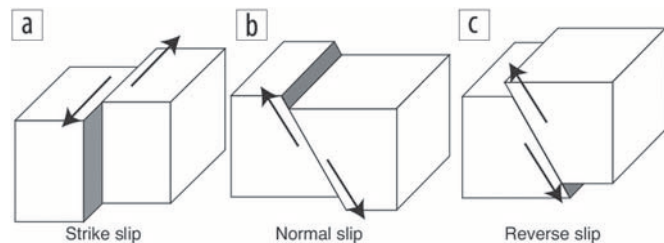


Figure 4. Three possible fault slip systems in a pure shear failure stress-strain regime.

often is annotated as σ_V , the maximum horizontal stress as σ_{H1} , and the minimum horizontal stress as σ_{H2} . A normal-slip stress regime occurs when $\sigma_V > \sigma_{H1} > \sigma_{H2}$, a strike-slip stress regime occurs when $\sigma_{H1} > \sigma_V > \sigma_{H2}$, and a reverse-slip stress regime occurs when $\sigma_{H1} > \sigma_{H2} > \sigma_V$.

Figure 5 shows diagrams of seismic source excitation caused by strike-slip faulting and a focal source mechanism “beach-ball” plot that illustrates the stress-strain changes. After faulting, the rock is either compressed or dilated, depending on its position relative to the motion along the fault (Figure 5b). Because of symmetry considerations, we cannot distinguish the fault and its auxiliary planes from the stress-strain changes alone. We need additional constraining information (e.g., from geology or geomechanics) to determine the actual plane on which the slip displacement occurred.

Conventionally, we represent the compression and dilation regions as black and white, respectively (Figure 5c). Hence, we can represent the faulting and focal source mechanism with a beach-ball plot (Figure 5d). The stress-strain changes radiate seismic energy, and based on the beach-ball plot, we can determine the source-radiation pattern of the seismic waves. (The small black arrows in Figure 5d are first ground-motion particle displacement vectors for a P-wave source-radiation pattern.) Therefore, if we have a dense array of geophones to record the seismic waves generated by a microseismic source, we can estimate the source mechanism from the polarity of P-wave first arrival. Interested readers can find a more detailed explanation of earthquake source mechanisms in Scholz (2002); Stein and Wysession (2003), Chapter 4; and Shearer (2009), Chapter 9.

If the microseismic rupture process is a pure shear failure (i.e., one of three types of faulting systems shown in Figure 4), we can represent the source mechanism as a simple double-couple (DC). In reality, the rupture process of a microseismic event likely will include some component of tensile failure because of the pore-pressure changes during fluid injection (red arrow in Figure 3). In this case, we need to consider all six independent stress components for the source moment tensor instead of only three. Microseismic source mechanisms are therefore, in general, a combination of a DC component plus a compensated linear vector dipole (CLVD) component and an isotropic (ISO) component (Figure 6). Note that even though the CLVD component for microseismic source mechanisms tends to be proportionally larger (as a result of fluid injection) than that of natural earthquakes, the DC component usually is still the dominant source mechanism.

Special section on microseismic source mechanisms

Our intent in creating this special section is to present a set of practical and informative technical articles that covers both the fundamentals and the current state of the art in microseismic source-mechanism analysis. In addition, we hope to highlight new and emerging source-mechanism concepts that are potentially important for a wide range of passive-monitoring applications, including groundwater, petroleum, geothermal, and CO₂ sequestration. We hope this special section will convey these new developments and capabilities to the

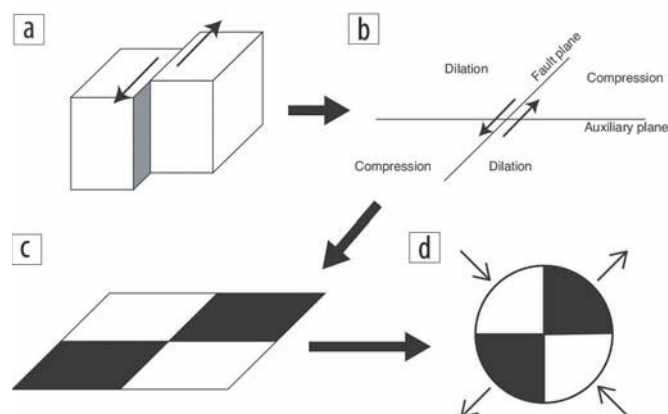


Figure 5. Diagrams to relate fault slip, seismic source mechanism, and the classic beach-ball plot: (a) fault slip, (b) stress-strain changes, (c) stress-strain changes (black is compression, white is dilation/tension), and (d) beach-ball plot showing the P-wave first-motion radiation pattern (small arrows are particle-displacement vectors).

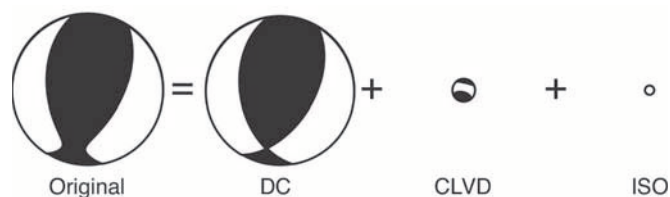


Figure 6. Example of a microseismic focal source mechanism (original) and its decomposition into double-couple (DC), compensated linear vector dipole (CLVD), and isotropic (ISO) source mechanism components. The size of each beach ball corresponds to the relative strength of each source-mechanism component.

broader geophysics community and will stimulate new ideas and research to address practical challenges that passive-seismic monitoring might solve.

To begin this special section, Eyre and van der Baan present moment-tensor inversion techniques to calculate seismic source mechanisms. They describe the benefits of moment-tensor inversion in microseismic monitoring and present an overview of the three common methods, including advantages and limitations.

Staněk et al. present a methodology to invert for the stress-field orientation from microseismic events induced during the hydraulic-fracture stimulation of shale gas reservoirs in North America. The inverted stress field is consistent with the regional stress and is determined from source-mechanism analysis of events monitored by a surface geophone array.

Rodríguez-Pradilla presents a passive-seismic monitoring case study for source characterization of microseismic events generated during a hydraulic-fracturing operation in a coalbed methane (CBM) reservoir in Colombia. Parameters of the fracking operation, such as the stimulated reservoir volume, state of stress of the reservoir, and failure mechanism of the microseismic events, are interpreted from the results of the hypocenter location and source-mechanism analysis.

Maxwell et al. discuss how microseismic geomechanical models can be used to examine reservoir deformation associated with hydraulic fracturing and predict various components of the

hydraulic-fracture system, including aseismic primary fractures and microseismicity resulting from various physical mechanisms. The authors describe an interpretation framework that integrates the 3D reservoir model, fracture engineering, and microseismic activity to better understand the mechanism of detected microseismic sources.

Baig et al. show that microseismic source mechanisms can be inverted for fracture orientations and, along with an assessment of overall rupture dimensions, can be used to construct a discrete fracture network (DFN) model. They present a methodology to use information from a subset of microseismic events for which source mechanisms can be determined to extend the DFN model across the reservoir area where events are detected.

Diller et al. examine some advantages of surface microseismic monitoring and suggest ways in which these advantages can improve the use and interpretation of microseismic data. In particular, they show methods that can increase the confidence in surface microseismic results, and they show that microseismic events with high-confidence locations and source mechanisms can be used to directly construct fracture networks.

Rutledge et al. present an interpretation of hydraulic-fracture microseismicity for cases in which persistent dip-slip

or strike-slip mechanisms exhibit shear planes prevalently aligned close to the principal-stress direction. They propose that the repetition of microseismic shearing events is driven by the strain of vertical hydraulic fractures propagating through the regular mechanical discontinuities of flat-lying stratigraphy.

Shuck et al. close this special section with a case history of a surface microseismic survey in a noisy environment. By use of a geophone patch geometry and careful data processing, source mechanisms are determined successfully for most identifiable events. **■**

References

- Scholz, C. H., 2002, *The mechanics of earthquakes and faulting*: Cambridge University Press, <http://dx.doi.org/10.1017/CBO9780511818516>.
- Shearer, P. M., 2009, *Introduction to seismology*: Cambridge University Press, <http://dx.doi.org/10.1017/CBO9780511841552>.
- Stein, S., and M. Wysession, 2003, *An introduction to seismology, earthquakes, and earth structure*: Wiley-Blackwell.